Mansoura University
Faculty of Engineering
Mansoura Engineering Journal

Investigation and Comparative Study of 12/16 C-core and Conventional Radial Flux Switched Reluctance Motor under Coil Fault Conditions

Mohamed Moustafa M. Sedky

KEYWORDS:
Switched reluctance motor, C-Core SRM, Radial Flux SRM, Axial flux SRM Fault analysis, Electrical vehicle, finite element analysis, failure coil

***Abstract*— Owing to the large quantity of conventional passenger vehicles with internal combustion engines, energy shortages and environmental pollution are now Seen as important problems. Electric vehicles (EVs) have the best energy savings and zero emission vehicles option. Radial Flux Switched Reluctance Motor (RFSRM), and Axial Flux Switched Reluctance Motor (AFSRM) have shown promise in wheel motor design of electric vehicles. While C-core is modelled, giving advantages of both radial and axial flux SRM. Based on a three-phase 12/16 pole structure, C-core RFSRM and conventional RFSRM are investigated and compared under different types of coils failures, while their impact on the average torque for both motors is presented. Comparisons of average torques at different coils` fault conditions between C-Core RFSRM, and conventional RFSRM have been done by finite element analysis (FEM). The segmental structure of C-Core RFSRM and its independent separate magnetic path for its coils, give it the superiority more than conventional RFSRM for in-wheel electric vehicle application.**

I. INTRODUCTION

THE major driving force in the development of electrical vehicles for urban transport is the environmental and economic issues. Traction motor selection is a key component of EV. With rapid transportation transition, it increases substantial awareness of the parameters used in the selection of motors. Switched Reluctance (SR) motors are currently used in a variety of applications in the sectors of EV, electrical aircraft, renewable energy, domestic appliances, and wind turbines [1,2]. Because of SRM provides simple structure, robustness, high starting torque, fault tolerance, high speed operation and low manufacturing costs [3-5], it has been considered fit for EV since 2000.

Comparison of various traditional and non-conventional electrical motors for EV applications is provided in [6]. The SR motor was used in hybrid electric vehicles [7]. SRM is preferred because the rotor side uses neither field windings nor PMs. Also, SRM is a low-cost motor and has rotor construction that is simple and durable compared to other electric motors. Because of its merits, it is suitable for harsh environments and safety-critical applications.

The influence of different stator pole and yokes shapes was investigated in [8,9], and a less vibration structure was proposed for 8/6 SRM. Greater torque was achieved through the topology of the shark pole surface and the design of the C-core stator in [10,11]. The duel rotor shaped topology is proposed in [12] with 20 percent increase in torque output, but with a bulky structure.

Received: (09 November, 2020) - Revised: (24 January, 2021) - Accepted: (07 February, 2021)

** **Corresponding author:** Mohamed Moustafa M. Sedky is a lecturer in the Department of Electrical Engineering, Faculty of Engineering, Alexandria University, he received the B.Sc. and M.Sc. degrees from Alexandria University, Alexandria, Egypt, in 1994 and 1999, respectively, and the Ph.D. degree from Heriot-Watt University, U.K in 2004, his current research interests include electric machines, electric drives, power, and power electronics. Mohamed.sedky@alexu.edu.eg.*

(Ser. No. BFEMU-2011-1072)

Up to now, the mechanical gear system has reduced the efficiency of 20 to 30 % in the EV application. As a solution to mechanical gear problem, the in-wheel engine technology has been introduced to the service and the engine is being developed with the new name of "outer rotor hub machine"[13,14]. In this configuration, the stator with its winding is located inside the outer rotor, but with drawbacks of poor heat dissipation because of the limited space for stator winding.

Due to a phase excitation, there is a torque ripples, so an axial flux SRM came into practical to minimize it [15, 16]. A novel prototype axial flux motor is developed in [17] towards the reduction of leakage flux. Various radial and axial flux design techniques for reducing torque ripple in SR machines have been discussed in [18-22].

A segmented SRM in-wheel axial-flux was suggested in [23]. A nonmagnetic, structural disk keeps the segments together. Two specially segmented rotors sandwich the stator, which are both mounted on nonmagnetic support plate. It was developed especially for direct drive motorcycles or light scooters. A doubly segmented axial flux SRM was also developed in [24]. That of the 12 C-shaped stator modules, directly mounted on the frame, have two attached coils together. The rotor consists of 8 active segment which is similarly moved. Because of the low iron and copper losses the highly compact system has good performance. A two-phase, axial flux, high-speed SRM with modular stator and twin segmented rotor was developed [25]. The SRM version proposed by in [26] is more complex, having more iron core but potentially more robust.

An axial flux C-core SRM is designed for in-wheel EV application in [27], and a novel approach to C-core radial flux SRM 12/15 is implemented in [28]. This structure is defined by an odd number of rotor poles. In-general odd number of rotor / stator poles is not desirable for traditional motor field structure because of unbalancing magnetic field, and it is a limitation of conventional radial field motor structure. A C-core RFSRM 12/16 is adapted in place of 12/15 in [29]. Where it offers shorter axial length. C-core RFSRM has the combined advantages of SRM radial and axial flux [30].

The effect of faulty coils on the transient performance of C-core and conventional RFSRM is investigated, and the comparison between the two types of machines has been done. The paper is arranged as follows: the SRM principles, 3D FEM modelling of C-Core RFSRM 12/16. Using Ansys FEM transient solver to investigate the behaviour of C-Core SRM at healthy and faulty conditions, comparing the impact of faulty coils on magnetic flux`s path and the transient response of C-Core SRM and conventional RFSRM at the same fault, with the same connection and drive circuit, then finally conclusion for the results.

II. PRINCIPLES OF SWITCHED RELUCTANCE MOTOR

SRM operating principle is to generate torque by varying magnetic reluctance. The SRM motor has double salience, meaning that it has both a saliency in the stator and a saliency in the rotor. Multiple SRM configurations can be constructed, depending on the rotor and stator pole number. The production of SRM torque is made by the tendency of the magnetic circuit to adopt a minimum reluctance configuration [30]. Torque production is independent of phase current direction, allowing the use of the unipolar power converters. As shown in Fig. 1, a conventional 12/16 RFSRM, coil is wound around each pole of the stator.

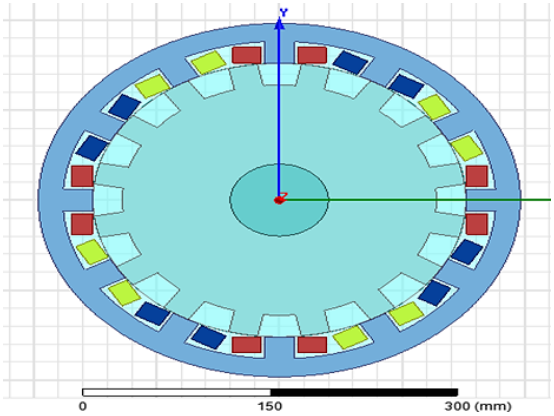

Fig. 1. Conventional RFSRM 12/16

The SRM's inductance, which is inversely proportional to reluctance, is dependent on the rotor displacement angle, θ, as illustrated in Fig. 2. The minimum inductance, L_u, occurs at the unaligned position and the maximum inductance, L_a, occurs at the aligned position. The idealized inductance profile for the phase winding as a function of the rotor displacement angle θ is shown in Fig.*2*, which is referenced with respect to the unaligned position. Neglecting the mutual inductance effect between phases, the general voltage equation of the SRM is

$$V = ir + \frac{\partial \Psi(\theta,i)}{\partial t} \quad \text{(V)} \qquad (1)$$

and the general expression for the instantaneous torque, using virtual work theory, is

$$T = \frac{1}{2} i^2 \frac{\partial L(\theta)}{\partial \theta} \qquad (2)$$

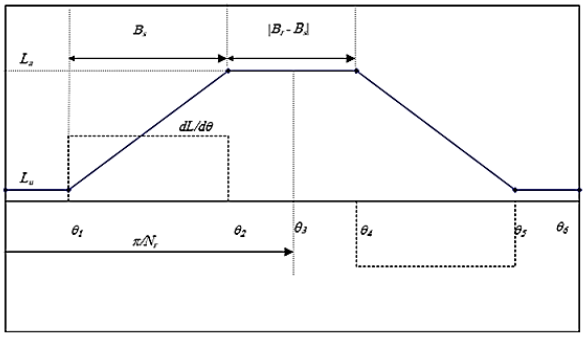

Fig. 2. Ideal SRM inductance profile

III. FEM OF C-CORE AND CONVENTIONAL RADIAL FLUX SWITCHED RELUCTANCE MOTOR

FEM 3D, 2D is used to model both the C-Core RFSRM 12/16, and conventional RFSRM 12/16. The modelling of C-core RFSRM 12/16 [30] is carried out using FEM, where the dimensions are shown in Table I. Steel 18 material is considered for both rotor and stator. The 3D FEM is shown in Fig.3, where the stator consists of 12 portable magnetic circuit.

TABLE I
C-CORE SRM DIMENSION

Ns, No. of poles in stator	12
Nr, No. of poles in rotor	16
q, phases numbers	3
Rotor`s outer diameter	304 mm
Rotor`s inner diameter	256 mm
Rotor`s pole pitch	22.5°
stator`s pole pitch	30°
Stator pole arc	9°
Rotor pole arc	9°
Stator core length, ls	105 mm
Stator core width, ws	100 mm
Rotor pole length	24 mm
Rotor pole width, w_{rp}	30 mm
Stator pole length, l_{sp}	10 mm
Stator pole width, w_{sp}	30 mm
No. of turns per pole	50 turn
Rated Speed, N	600 RPM
Rated current, I	40 A
Input voltage, V	220 V

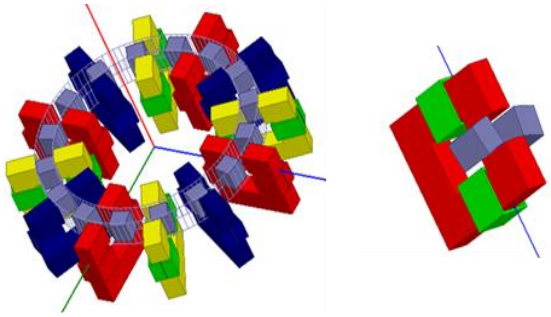

Fig. ٣. 3D FEM geometric of 12/16 C-Core SRM

The 12 cores of stator are having individual three phase windings; each winding is consisting of four coils connected in parallel. The 2D FEM of each core is shown in Fig.4. The compared conventional RFSRM 12/16, Fig.1, is modelled with the same outer-diameter, air gap length, rotor pole arc, stator pole arc, same material, and the same axial length. Special care must be taking in assigning the FEM mesh, due to the dynamic modelling and longtime simulation.

FEM transient model is used to investigate the motor performance at different faulty scenario. The aim of transient study is to investigate the percentage drop of generated torque at different faulty coil`s conditions, and different speed.

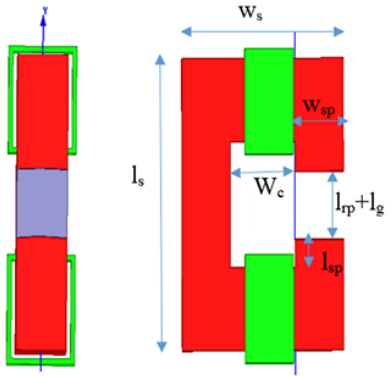

Fig. ٤. 2D geometric of C-Core SRM single segment

At rotor position θ, the magnetic flux density of each element is calculated by ANSYS software of FEM, and hence, the magnetic co energy *W′(θ)*. Inductance, L(θ), in rotor position θ is calculated according to the following equation.

$$L(\theta) = \frac{2w'(\theta)}{i^2} \quad (3)$$

Using *L(θ)*, the development torque *T(θ)* is calculated according to eq. (1).

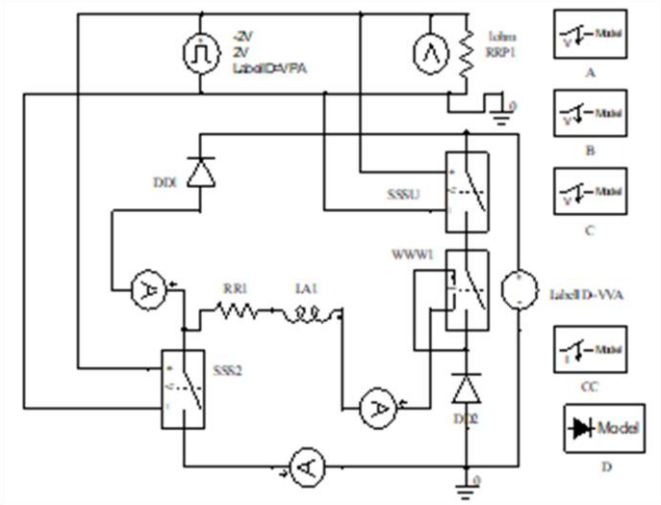

Fig. ٥. Drive circuit for transient simulation of FEM for one coil

To investigate the effect of each coil's fault, so each coil has to be excited separately. While one coil`s drive circuit for transient analysis is shown in Fig. 5. Because of paralleling coils, each phase consists of four drive circuits, where there are 12 separates driving circuit for the three phases machine.

The four coils for each phase are connected in parallel. Paralleling of phases' coils gave the merit of investigating the output performance at different scenario of faulty cases. For complete faulty phase, four coils should be faulty together. Due to paralleling, each phase could have one faulty coil or more by open circuit its drive circuit. Different scenarios are listed in Table II, which will be applied for the two types of machines.

TABLE II
Faulty coils scenarios

Type of fault	Scenario 1	Scenario 2	Scenario 3	Scenario 4
1 coil	1 in A	1 in B	1 in C	
2 coils	2 in A	1 in A 1 in B	1 in A 1 in C	1 in B 1 in C
3 coils	3 in A	2 in A 1 in B	1 in A 2 in B	1 in A 1 in B 1 in C
4 coils	4 in A	3 in A 1 in B	2 in A 2 in B	1 in A 3 in B

IV. C-CORE RFSRM FAULTY CONDITIONS

The aligned and unaligned inductances for each coil of C-Core SRM, are 1.625 mH, and 0.875 mH, respectively. Under constant speed of 600 RPM, and maximum coil current 40 A, the flux linkage current distribution for different scenarios, is

shown in Fig. 6, which represents the co-energy area for each case. Where all scenarios for each fault type are giving the same results.

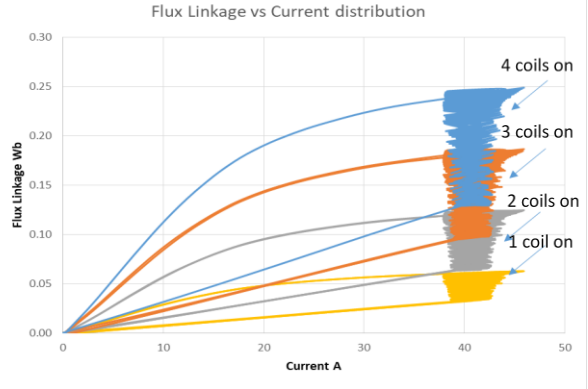

Fig. ٦. Flux linkage / current distribution

The enclosed area is increased with increasing the number of healthy coils. Transient analysis of FEM 3D is used to find the average output torques at different types of faults. The duty angle is constant in all the scenario for 7.5º, which was found to give maximum output for healthy case. Average torque at different types of fault are listed in Table III.

TABLE III
Average torque distribution for C-Core RFSRM at different fault scenarios

Speed RPM	Healthy case	1 faulty coil	2 faulty coils (A1, A3)	2 faulty coils (A1, A2)	3 faulty coils	4 Faulty coils
300	34.5	30.6	27.5	28.1	25	22
600	34.2	30.6	27.4	28	24.9	22
1000	34.1	30.6	27.3	27.9	24.8	22.1
2000	33.9	30.5	27.3	27.9	24.8	22.1
3000	16.3	15.5	14.2	14.8	13.3	10.9
5000	11.5	9.3	8.9	9.1	7.9	6.5

From Table III for complete cycle is reduced by the percentage of sharing the faulty coils with respect to all coils. The average torque with respect to speed at different types of fault is in Fig.7.

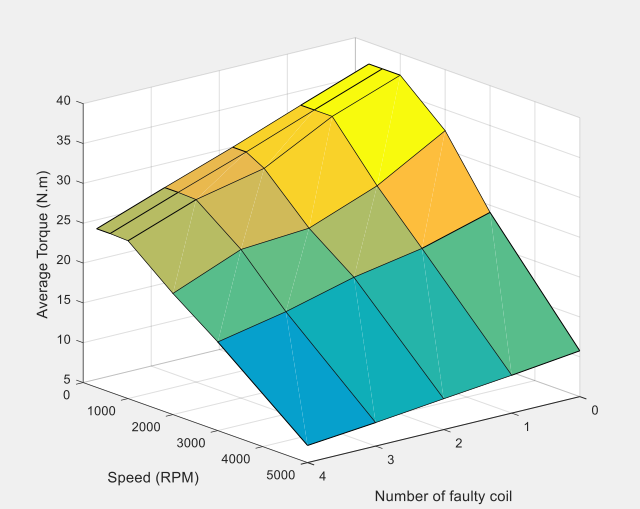

Fig. ٧. Average torque distribution at different speed, and different faulty scenario for C-Core SRM

It is shown that, the average torque is nearly constant for speeds below than 2000 RPM, and the average torque is reduced linearly with increasing the numbers of faulty coils. Reducing the average torque with increasing the number of faulty coils is not depending on the location of the faulty coils, but it is depending only on their numbers.

In C-core machine, each coil has its own flux path, which eliminates the magnetic coupling between phases even between coils in the same phase. The magnetic path for C-Core RFSRM one segment is shown in Fig. 8 [30].

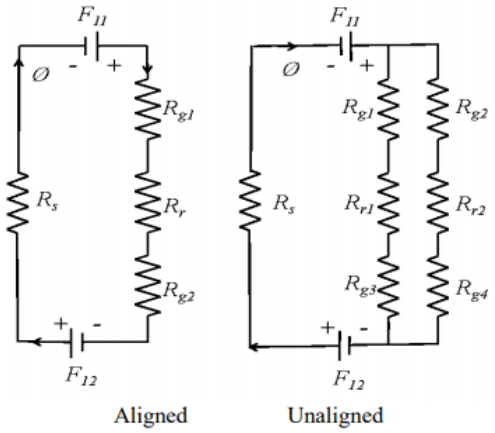

Fig. ٨. Magnetic flux's path for C-Core SRM one segment

The 3D magnetic flux distribution for one stator core is shown in Fig. 9(a, b) which proves the independency for each magnetic path. 3D Flux density distribution for healthy phase A is shown in Fig. 10(a, b). 3D flux density distribution for phase A, under the type of one faulty coil, is shown in Fig, 11(a, b), which shows the independency of each stator's core. Similarly, the 3 D flux density distribution for phase A, under the type of two faulty coils, (180º apart or consequences) are shown in Fig.12(a, b), and Fig.13(a, b), where there is no differences in the flux distribution for both cases. Because of independency of each stator core, so there is no difference if the two faulty coils are consequences or 180º apart. Each coil has its own path in stator and rotor teeth, without interface with the other stator segment. This gives the merit of the average development torque to be linear proportional with the number of healthy coils.

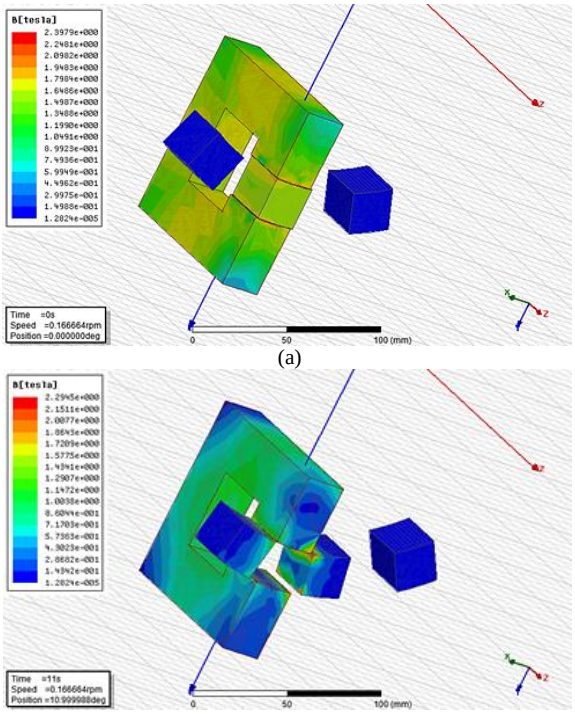

Fig. ٩. 3D flux density distribution for one stator core.
(a) aligned and (b) unaligned position

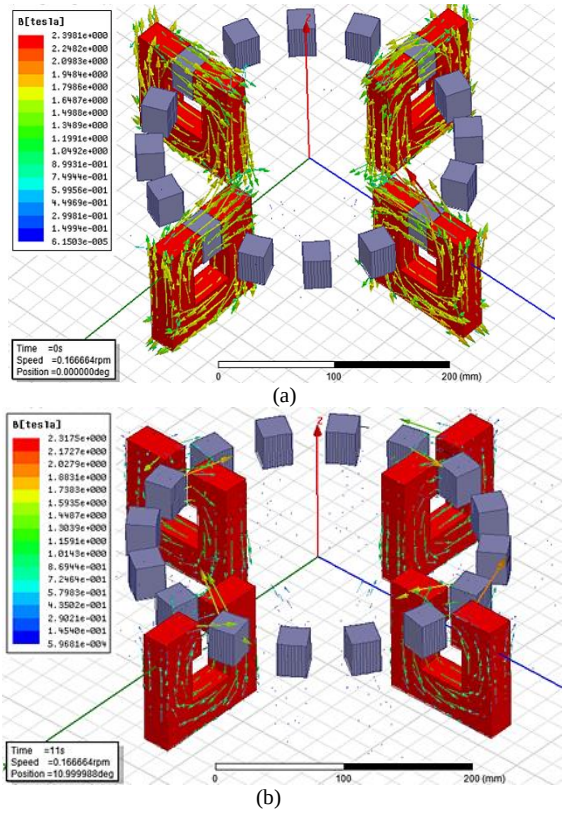

Fig. 10. 3D flux density distribution for healthy phase.
(a) aligned and (b) unaligned position

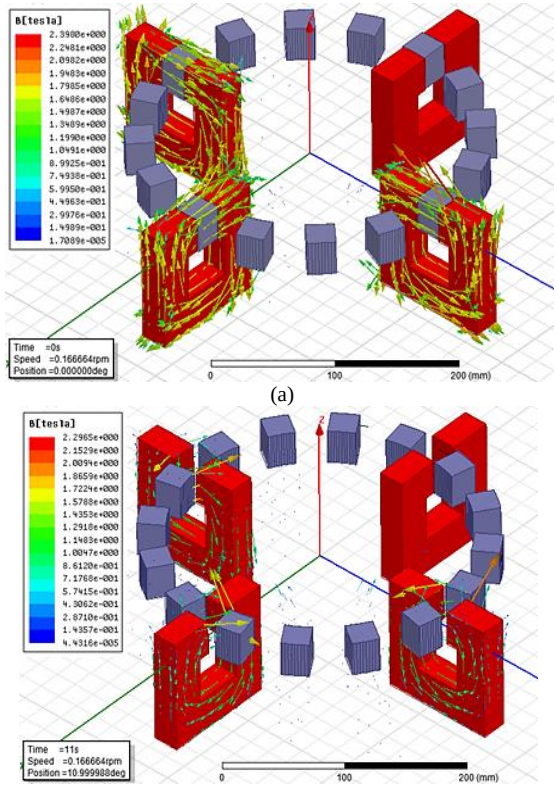

Fig. 11. 3D flux density distribution for 3 healthy coils and 1 faulty coil; (a) aligned and (b) unaligned position

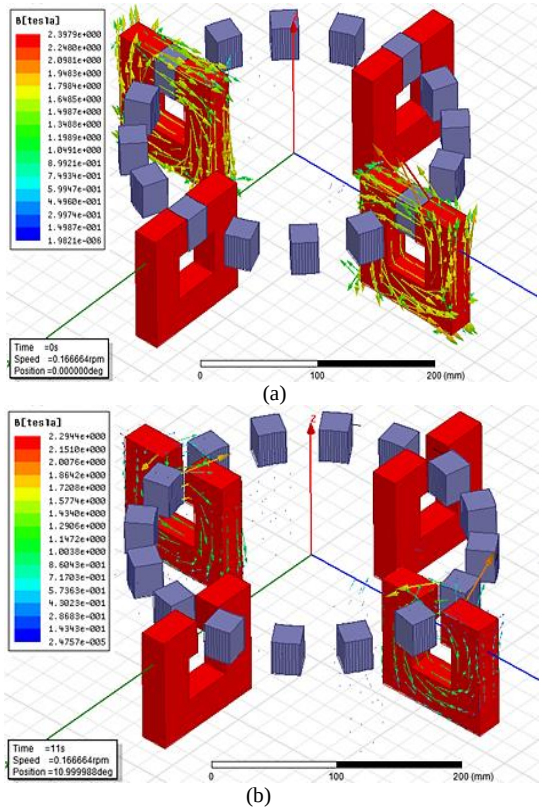

Fig. 12. 3D flux density distribution for 2 healthy coils and 2 faulty coils (180° apart); (a) aligned and (b) unaligned position

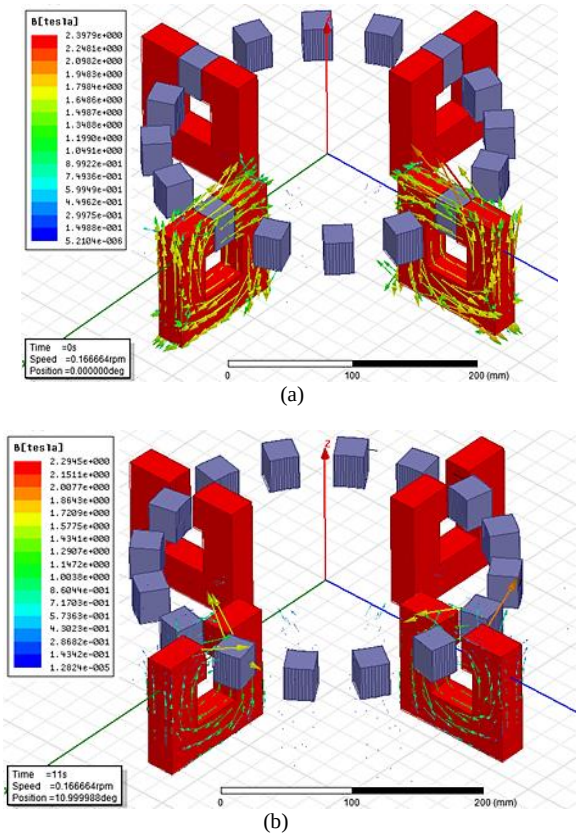

Fig. 13. 3D flux density distribution for 2 healthy coils and 2 faulty coils (consequence); (a) aligned and (b) unaligned position

V. CONVENTIONAL RFSRM FAULTY CONDITIONS

A conventional RFSRM 12/16 is compared with the C-Core RFSRM 12/16, which is having the same dimensions for outer, and inner diameter for both stator and rotor. The same materials are also used, and the same stator and rotor teeth angles are applied. The same driving circuits are used in the transient response. For transient analysis, the average torque with respect to speed at different fault scenarios, listed in Table II, is listed in Table IV. The average torque is shown in Fig. 14, where the average torque is not reduced linearly with the same percentage with the number of faulty coils, as it is proved in C-Core RFSRM.

The torque comparison for two faulty coils is shown in Fig.15, which illustrated the effect of location of faulty coil on the average torque. For two faulty coils in one phase, there are two cases, case (1); A1, and A2 are faulty, case (2); A1 and A3 are faulty. The two cases have different instantaneous and average torque, as shown in Fig.15. This is due to the difference of magnetic flux's path in each case. The magnetic flux path for conventional RFSRM healthy case is shown in Fig.16. The reluctance of the rotor pole, air-gap, yoke, and stator pole for the flux path are denoted by R_r, R_g, R_y, R_s respectively. This magnetic path is valid for all faulty scenario after replacing the faulty coil by zero ampere turn in Fig.16. Faulty coil in phase A is represented by zero F1. Two faulty coils (A1A2) are represented by zero (F1, F2) ampere turn, or (A1A3) are represented by zero (F1, F3) ampere turn. The three faulty coils scenario could be represented by zero (F1, F2, and F3) ampere turn.

TABLE IV
Average torque distribution for conventional RFSRM at different fault scenarios

Speed RPM	Healthy case	1 faulty coil	2 faulty coils (A1, A3)	2 Faulty coils (A1, A2)	3 faulty coils	4 faulty coils
300	34.5	30.6	27.5	28.1	25	22
600	34.2	30.6	27.4	28	24.9	22
1000	34.1	30.6	27.3	27.9	24.8	22.1
2000	33.9	30.5	27.3	27.9	24.8	22.1
3000	16.3	15.5	14.2	14.8	13.3	10.9
5000	11.5	9.3	8.9	9.1	7.9	6.5

The location of faulty coil has an impact on the average torque, due to the difference in magnetic path for each location.

The 2D magnetic flux distributions generated by FEM transient condition are shown in Fig.17-21 (a, b) for different scenarios. There is a symmetrical path for each coil in healthy case Fig. 17(a, b). The magnetic flux distribution for one faulty coil is not symmetrical around the axis as shown in Fig.18(a, b). The two faulty coils scenario has two cases, which each case has its magnetic flux distribution as shown in Fig.19-20(a, b). Where, in Fig.19(a, b) the flux distribution, is not the same as in Fig.20(a, b) for both aligned and unaligned position. The flux distribution for three faulty coils in phase A is shown in Fig.21 (a, b), where there is no symmetrical. Three faulty coils case is considered as a complement of 1 faulty coil.

The transient analysis at different speed and faulty scenario proves that, C-Core has independent stator cores, and the loss of average generated torque could be expected, which depends only on the number of faulty coils regardless their location. the comparison of percentage of normalized torque for C-Core and conventional RFSRM at different faulty coils and speed 600 RPM is shown in Fig.22. The percentage normalized torque of C-Core RFSRM is nearly matched with the theoretical curve, where the average torque depends on the number of remaining healthy coils. While for conventional RFSRM, the percentage normalized torque is less than the theoretical one by nearly 5 % and depends on the location of faulty coils (A1A2 or A1A3).

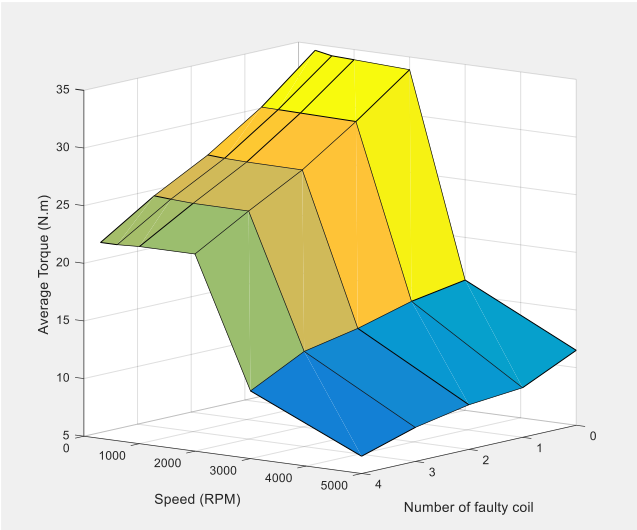

Fig. 14. Average torque distribution at different speed, and different faulty scenario for conventional RFSRM

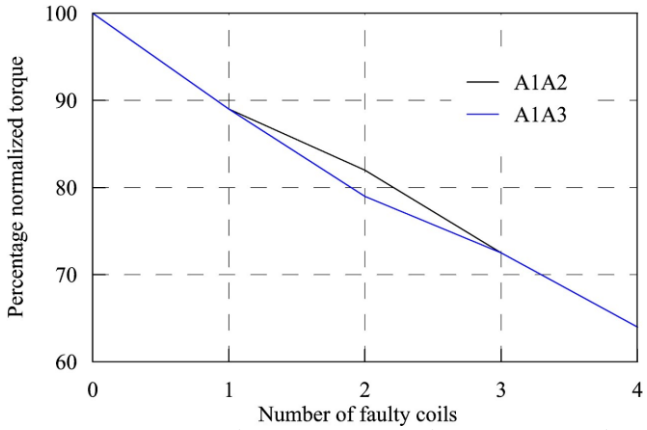

Fig. 15. Normalized torque for two cases (A1, A2 faulty coils, A1, A3 faulty coils)

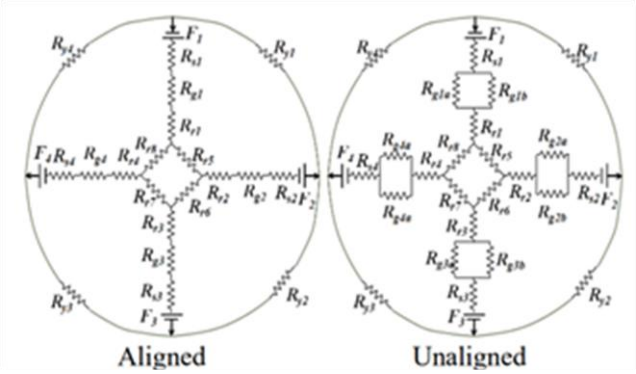

Fig. 16. Magnetic flux's path for RFSRM; healthy case

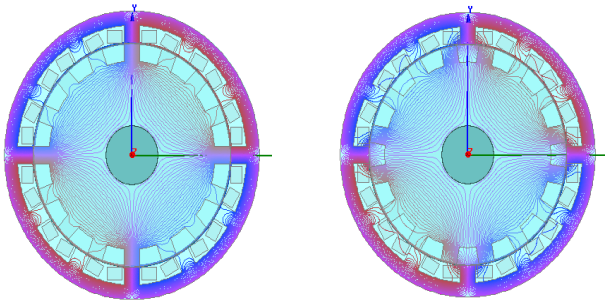

Fig. 1ᵛ. 2D Magnetic flux distribution for healthy phase; (a) aligned and (b) unaligned position

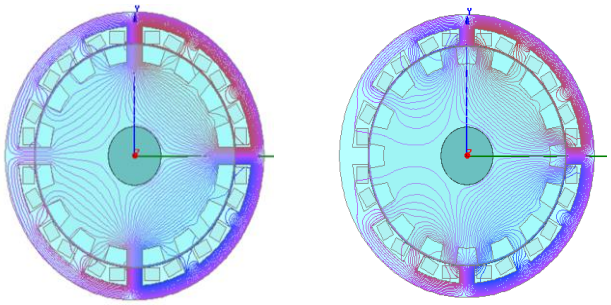

Fig. 18.2D Magnetic flux distribution for one faulty coil; (a) aligned and (b) unaligned position

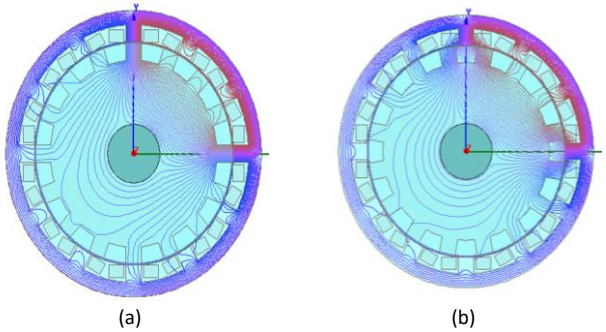

Fig. 19. 2D Magnetic flux distribution for two faulty coils (A1A2); (a) aligned and (b) unaligned position

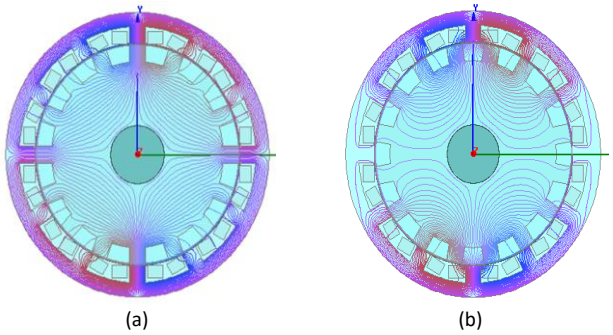

Fig. 20. 2D Magnetic flux distribution for two faulty coils (A1A3); (a) aligned and (b) unaligned position

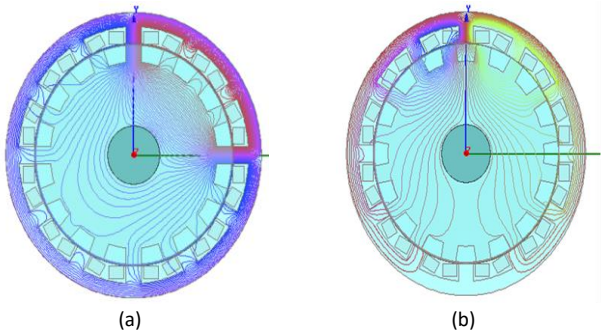

Fig. 21. 2D Magnetic flux distribution for 3 faulty coils; (a) aligned and (b) unaligned position

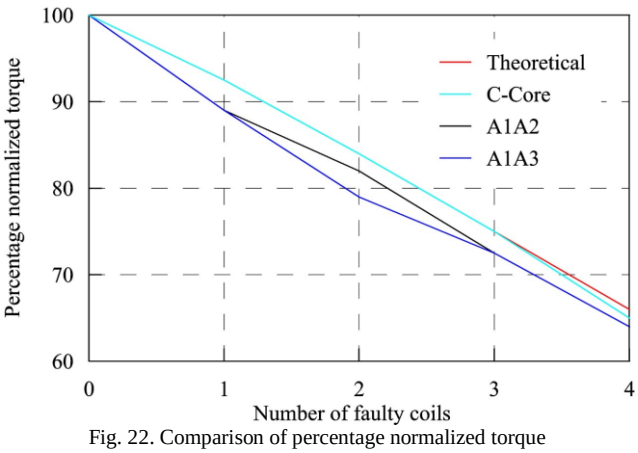

Fig. 22. Comparison of percentage normalized torque

VI. CONCLUSIONS

C-Core RFSRM has more reliability than the conventional RFSRM which was proved by 3D, and 2 D transient analysis by using FEM. The average torque of C-Core RFSRM 12/16 is linearly related to the number of healthy coils in each phase, and the magnetic flux's path is not disturbed for the healthy coils, while it is not the same in conventional RFSRM.

In C-Core RFSRM, average torque is not depending on the location of faulty coil, rather than it is depending only on the number of faulty coils. In conventional RFSRM, the average torque is not depending only on the number of faulty coils, but also on the location of the faulty coils to each other. This is because of the un-symmetrical magnetic flux`s path for the conventional RFSRM under fault conditions, unless the number of faulty coils are even and 180^{o} between them. The modular design of the C-Core RFSRM allows easy manufacturing as well as fast replacement of the damaged modules in the event of a coil failure. The downside of this approach is that it needs converters as many as coils. The individually of magnetic path for each coil in C-Core RFSRM gave it a potential candidate for electrical vehicle application.

REFERENCES

[1] T. J. E. Miller, "Optimal Design of Switched Reluctance Motors," IEEE Trans. Ind. Electron., Vol. 49, No.1, pp. 15–27, Feb. 2002.

[2] A. L. M. d. Santos, J. Anthonis, F. Naclerio, J. J. C. Gyselinck, H. V. d. Auweraer, and L. C. S. Goes, "Multiphysics NVH Modeling: Simulation of A Switched Reluctance Motor for an Electric Vehicle," IEEE Trans. Ind. Electron., Vol. 61, No. 1, pp. 469–476, 2014.

[3] M. Takeno, A. Chiba, N. Hoshi, S. Ogasawara, M. Takemoto, and M. A. Rahman, "Test Results and Torque Improvement of the 50-kW Switched Reluctance Motor Designed for Hybrid Electric Vehicles," IEEE Trans. Ind. Appl., Vol. 48, No. 4, pp. 1327–1334, 2012.

[4] H. Chen and J. J. Gu, "Switched Reluctance Motor Drive with External Rotor for Fan in Air Conditioner," IEEE/ASME Trans. Mechatronics, Vol. 18, No. 5, pp. 1448–1458, 2013.

[5] V. Valdivia, R. Todd, F. J. Bryan, A. Barrado, A. Lazaro, and A. J. Forsyth, "Behavioral Modeling of a Switched Reluctance Generator for Aircraft Power Systems," IEEE Trans. Ind. Electron., Vol. 61, No. 6, pp. 2690–2699, 2014.

[6] W. Xu, J. Zhu, Y. Guo, "Applied Superconductivity and Electromagnetic Devices," Proceedings of 2009 IEEE International Conference on Chengdu China, Sept., 2009.

[7] Lovatt, H.C. "Optimization of Switched Reluctance Motors for Hybrid Electric Vehicles," Power Electronics, Machines and Drives, International Conference, Publ. No. 487, pp. 177 – 182, 2002.

[8] J. Hong "Stator Pole and Yoke Design for Vibration Reduction of Switched Reluctance Motor," IEEE Trans. on Magn., Vol. 38, No. 2, pp.929-932, 2002.

[9] Jian Li, Xueguan Song, "Comparison of 12/8 and 6/4 Switched Reluctance Motor: Noise and Vibration Aspects," IEEE Trans. on Magn., Vol. 44, N0. 11, pp. 4131 - 4134, 2008.

[10] J. Corda, A.M. Tataru, P.O. Rasmussen and E. Ritchie, "Analytical Estimation of Torque Enhancement of the SR Machine with Saw-Shaped (Shark) Pole Surfaces," IEE Proc.-Electr. Power Appl., Vol. 151, No. 2, pp.223-229, 2004.

[11] Sh. H. Mao, M. Ch. Tsai, "Novel Switched Reluctance Motor with C-Core Stators" IEEE Transactions on Magn, Vol. 41, No. 12, pp. 4413-4420, 2005.

[12] W. Yang, "Design and Research of a New Dual Rotor Switched Reluctance Motor for Hybrid Electric Vehicles," Electrical Machines and Systems (ICEMS), International Conference, pp. 829 – 833, 2010.

[13] W. Yaling, "Outer-rotor Switched Reluctance Motor and Its Control System Used in Electric Vehicles", Electrical Machines and Systems (ICEMS), International Conference, pp. 1 – 4, 2011.

[14] Sakthivel, P., "Design of a 250 w, Low Speed Switched Reluctance Hub Motor for Two Wheelers," Electrical Energy Systems (ICEES), 1st International Conference, pp. 176 – 181,2011.

[15] R. Madhavan and B.G. Fernandes, "A Novel Technique for Minimizing Torque Ripple in Axial Flux Segmented Rotor SRM," IEEE Conference, Energy Conversion Congress and Exposition (ECCE), pp. 3383 – 3390, 2011.

[16] B. G. Fernandes, "A Novel Axial Flux Segmented SRM for Electric Vehicle Application," XIX International IEEE Conference on Electrical Machines – ICEM, pp 1-6. Sept. 2010.

[17] A. Labak, N. C. Kar, "Novel Approaches Towards Leakage Flux Reduction in Axial Flux Switched Reluctance Machines" IEEE Trans. on Magn, Vol. 49, No. 8 pp. 4738-4741, Aug. 2013.

[18] Y. Takano, A. Chiba, M. Takeno, T. Imakawa, N. Hoshi, M. Takemoto, and S, Ogasawara, "Torque Density and Efficiency Improvements of a Switched Reluctance Motor Without Rare-Earth Material for Hybrid Vehicles," IEEE Trans. Ind. Appl., vol. 47, no. 3, pp. 1240–1246, 2011.

[19] Y. K. Choi, H. S. Yoon, and C. S. Koh, "Pole-shape Optimization of a Switched-Reluctance Motor for Torque Ripple Reduction," IEEE Trans. Magn., Vol. 43, No. 4, pp. 1797–1800, Apr. 2007.

[20] J. Li, X. Song, and Y. Cho, "Comparison of 12/8 and 6/4 Switched Reluctance Motor: Noise and Vibration Aspects," IEEE Trans. Magn., Vol. 44, No. 11, pp. 679–686, 2008.

[21] A. Siadatan, E. Afjei, "An 8/6 Two Layers Switched Reluctance Motor: Modeling, Simulation and Experimental Analysis" Majlesi Journal of Electrical Engineering, Vol. 6, No. 1, pp.1-10,2012.

[22] T. Higuchi, K. Ueda, and T. Abe, "Torque Ripple Reduction Control of a Novel Segment Type SRM with 2-steps Slide Rotor," in Proc. IEEE Int. Power Electron. Conf., pp. 2175–2180,2010.

[23] P. Andrada, E. Martínez, M. Torrent, B. Blanqué, J.I. Perat, "Novel in wheel axial-flux segmented switched reluctance motor," in Proceedings of the 19th European Conference on Power Electronics and Applications (EPE '17 ECCE Europe), Warsaw (Poland), 2017.

[24] Z. Pan, S. Song, R. Ma, "A novel axial flux switched reluctance machine with segmented stator and rotor," in Proceedings of the 20th International Conference on Electrical Machines and Systems (ICEMS '2017), Sydney (Australia), 2017.

[25] J.H. Potgieter, F.J. Márquez-Fernández, A.G. Fraser, M.D. Mc Culloch,"Performance evaluation of a high speed segmented rotor axial flux switched reluctance traction motor," in Proceedings of the 22nd International Conference on Electrical Machines (ICEM '2016), pp. 531-537, 2016.

[26] W. Ding, Y. Hu, T. Wang, S. Yang, "Comprehensive research of modular E-core stator hybrid-flux switched reluctance motors with segmented and non-segmented rotors," IEEE Transactions on Energy Conversion, vol. 32, No. 1, pp. 382-393, 2017.

[27] B. Bilgin, A. Emadi, and M. Krishnamurthy, "Comprehensive Evaluation of the Dynamic Performance of a 6/10 SRM for Traction Application in PHEVs," IEEE Trans. Ind. Electron., Vol. 60, No. 7, pp. 2564–2575, 2013.

[28] Nikunj R. Patel, Varsha A. Shah, and Makarand M Lokhande "Design and Performance Analysis of Radial Flux C-Core Switched Reluctance Motor for In-Wheel Electrical Vehicle Application," IEEE ITEC Conference, pp 1– 6, June 2016.

[29] Nikunj R. Patel, Varsha A. Shah, and Makarand M Lokhande "A Novel Approach to the Design and Development of 12/15 Radial Field C-core Switched Reluctance Motor for Implementation in Electric Vehicle Application," IEEE Transactions on Vehicular Technology, 2018.

[30] N. Patel, V. Shah, and M. Lokhande, "Comparative Analysis of 12/16 Conventional and Proposed C-core Radial Flux SRM Topologies for In-wheel Electric Vehicle Application", Majlesi Journal of Electrical Engineering, Vol. 13, No. 2, pp. 57-65, 2019.

Title Arabic:

(التحرى والدراسة المقارنة لمحرك الممانعه بتبديل التدفق الشعاعي١٢/١٦ ذو قالب سى ولمحرك تقليدي في حالات عطل الملف)

Arabic Abstract:

:- تعتبر زياده السيارات ذات الاحتراق الداخلى ونقص الطاقه وتلوث البيئه من اهم المشكلات. ولذلك للسياره الكهربيه الفضل في حفظ الطاقه وانعدام الانبعاث. وقد اثبتت

ايجاد العزوم الناتجه في كل حاله من الاعطال ومقارنتها عند سرعات مختلفه . وقد ظهر من الدراسه والمقارنه ان الهيكل المقطعى لمحرك الممانعه التبادليه ذو القلب على شكل حرف سى يمنح الاستقلاليه في مسارات تدفق المجال المغناطيسى في حالات العطل وعدم العطل سواء. وايضا نسبه الفاقد في معدل العزم يتناسب طرديا مع عدد الملفات اللتى بها عطل وتعتبر هذه ميزه من مميزات هذا النوع من المحركات.

محركات الممانعه التبادليه ذو التدفق الاشعاعى والمحورى مميزات في تصميم اطارات السيارات الكهربيه. بناء على ذلك تم دراسه ومقارنه بين نوعين من محركات الممانعه التبادليه ثلاثى الاوجه ١٢/١٦، احدهما تقليدى والاخر ذو قلب على شكل حرف سى، وكلاهما ذو تدفق اشعاعى. تمت المقارنه والدراسه عند حالات مختلفه من عطل الملفات وتمت الدراسه باستخدام برنامج العناصر المحدده الثلاثى والثنائى الابعاد. تم دراسه مسارات تدفق المجال المغناطيسى في كل حاله من الاعطال مع نوعى المحركات و تم ايضا